GLOBAL NITROUS OXIDE ASSESSMENT

N_2O

SUPPLEMENTARY INFORMATION

Table of Contents

SI 2 Nitrous oxide sources and trends

SI 2.1 Nitrous oxide emission estimation techniques

Bottom-up techniques

Nitrous oxide fluxes can be measured on scales of one to hundreds of metres using flux chambers and eddy covariance measurements, respectively (Butterbach-Bahl *et al.* 2013). Flux chambers are the most common method and consist of a closed chamber from which air is sampled and its concentration is determined using a nitrous oxide analyser. Flux chambers can be used to precisely measure the impact on fluxes from different management or the influence of different soil and/or vegetation. The main drawback of this method is that only a very small area is sampled, while nitrous oxide fluxes are known to be very heterogeneous in space and time consisting of hot spots and hot moments (Ball *et al.* 2000; Butterbach-Bahl *et al*. 2002). Eddy covariance measurements are made by analysing nitrous oxide concentrations in upward as opposed to downward moving parcels of air in near-surface atmospheric eddies. The flux of nitrous oxide can be derived from the difference in concentrations between these air parcels. Fluxes determined with this method cover an area on the order of 1 hectare and thus are more representative of a field or ecosystem than flux chambers (Eugster *et al.* 2007). Even with this method, however, it is not possible to have complete coverage of a given landscape let alone a country. For this reason, it is necessary to scale-up these local measurements to derive an estimate at landscape, country or even global scale. This can be done using empirical models or inventories, which rely on the relationship of nitrous oxide fluxes to various environmental and/or land management parameters, such as soil temperature, soil moisture and nitrogen input (Butterbach-Bahl *et al.* 2013). Alternatively, these measurements can be used to develop and/or calibrate process-based models, which parameterise nitrous oxide fluxes as a function of various environmental parameters (Tian *et al.* 2019).

Top-down techniques

Nitrous oxide fluxes can be determined using measurements of it in the atmosphere and a model of the relationship between changes in atmospheric concentration and fluxes. This may be a simple, for example a 1-box model, or a 3D atmospheric chemistry transport model (Huang *et al.* 2008; Saikawa, Schlosser and Prinn 2013; Thompson *et al.* 2014). This method is referred to as top down. When 3D models are used, the spatial and temporal distribution of nitrous oxide in the atmosphere can provide information on the magnitude and distribution of the fluxes. In this case, the fluxes are determined through a method called atmospheric inversion. In atmospheric inversions, the mathematical problem to determining the fluxes is under constrained, therefore, statistical optimisation methods are used to find the most probable estimate of nitrous oxide fluxes, that is, the one that best fits the observations while being constrained by some prior estimate of the fluxes.

Measurements of nitrous oxide in air can be made using several methods. The first measurements available were made using gas chromatographs (GC) which separate nitrous oxide from the other components of air and determine the quantity of nitrous oxide using an electron capture detector (Weiss, 1981). Over the last two decades, spectroscopic methods have been developed that have the precision necessary to resolve

small variations in atmospheric nitrous oxide. These include quantum cascade laser absorption spectrometry (QCLAS) in which light can be produced with a very narrow wavelength range to target specific absorption bands and can be used for open or closed path spectroscopy (Eugster *et al.* 2007). For closed path spectroscopy, the signal-to-noise ratio has also been enhanced by using spectroscopic methods that essentially increase the absorption path length, such as cavity ring-down spectroscopy (CRDS) and integrated cavity output spectroscopy (ICOS). Such spectroscopic instruments are available commercially and are replacing GCs because of their increased stability and lower maintenance requirements (Lebegue *et al.* 2016). These instrumentation methods can be used to determine the amount of nitrous oxide in air samples taken at ground-based monitoring sites, such as in the Global Monitoring Laboratory network of National Oceanic and Atmospheric Administration (NOAA) or the Advanced Global Atmospheric Gases Experiment (AGAGE) network), from aircraft or balloons.

Satellite observations are not currently used to detect nitrous oxide sources or to derive emissions because the measurement of nitrous oxide is more challenging than for the other long-lived greenhouse gases owing to its weak spectral signature in the infrared range and its relatively low variability in the troposphere (Chalinel *et al.* 2022). There are, however, ongoing efforts to retrieve nitrous oxide from existing satellite instruments. Retrievals have, for example, been made using measurements from the infrared atmospheric sounder interferometer (IASI) on the Metop-A satellite and have achieved a random error on a single retrieval of total column nitrous oxide of around 2 ppbv and a bias compared to aircraft profiles of nitrous oxide of about 1 ppbv; however, these errors are still large compared to the variability of nitrous oxide in the troposphere (Chalinel *et al.* 2022). Retrievals have also been made using measurements from the thermal and near infrared sensor for carbon observation (TANSO) on the GOSAT satellite, but similar levels of uncertainty are obtained as with IASI (Kangah *et al.* 2017).

Uncertainties of bottom-up as opposed to top-down techniques

Each of the two emission estimation approaches, bottom up and top down, are associated with their own distinct sources of uncertainties. The main source of uncertainty in inventory-based estimates, a bottom-up approach, is in the relationship between nitrous oxide emission and nitrogen input, that is the emission-factors (EFs). These do not fully capture the dependence of nitrous oxide emissions on land management, vegetation or the physical and biochemical properties of soils and thus do not capture the spatial and temporal heterogeneity of the emissions (Tian *et al.* 2019). Furthermore, they are typically used to describe a linear relationship between nitrous oxide emissions and nitrogen inputs, however, in soils with very high nitrogen inputs the response can be greater than linear (Shcherbak, Millar and Robertson 2014; Cui *et al.* 2021). For such cases, an alternative approach has been proposed using nitrogen balance, i.e., the balance between nitrogen inputs and the nitrogen removed in crops, which is thought to better predict nitrous oxide as it reflects the importance of NUE for nitrous oxide emissions but is only applicable to direct emissions from croplands (Eagle *et al.* 2020). Process-based models, another bottom-up method, have uncertainties mainly stemming from approximations and assumptions made in the process parameterisations as well as from missing processes and information (Tian *et al.* 2019). The largest uncertainties in top-down methods, namely, atmospheric inversions, are due to errors in the modelled atmospheric transport and the dependence on the prior flux estimate, which is governed by the number of observation sites and the observation frequency (Tian *et al.* 2024).

Despite these uncertainties, there is good agreement between top-down and bottom-up estimates for total nitrous oxide emissions at global and regional scales, lending confidence in the ability of both methods to accurately estimate the emissions at fairly large scales (Tian *et al.* 2024).

SI 2.2 Nitrous oxide emissions and regions

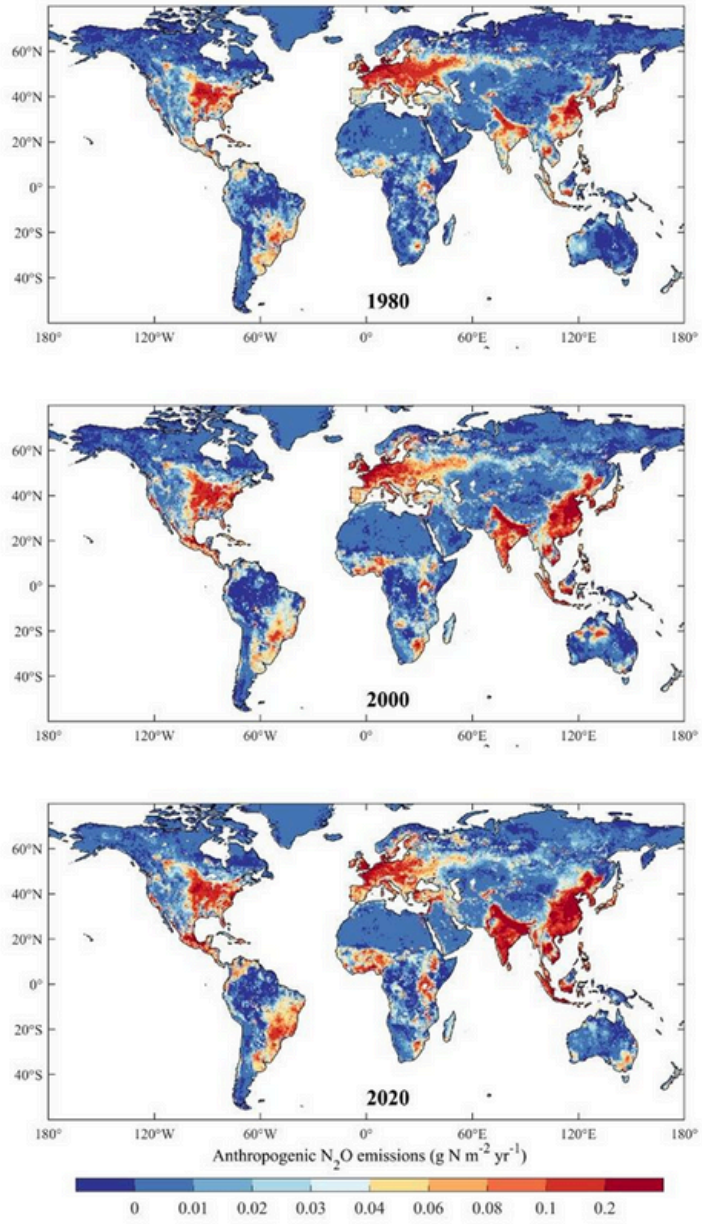

Figure SI 2.1 *Anthropogenic emissions of nitrous oxide, 1980 (top), 2000 (middle) and 2020 (bottom), grams of nitrogen per square metre per year*

Table SI 2.1 *Regional definitions used in Chapter 2. The regions are defined considering the similarity of the country-level nitrous oxide emission trend and economic development situation, while keeping each region contiguous.*

Region name	Region description	Countries or territories
North America	Wealthy countries with little change in emissions.	Bermuda Islands, Canada, United States of America (with Alaska)
Central America	Developing economies with slightly increasing agricultural emissions.	Anguilla, Antigua and Barbuda, Bahamas (the), Barbados, Belize, British Virgin Islands, Cayman Islands, Costa Rica, Cuba, Dominica, Dominican Republic (the), El Salvador, Guadeloupe, Guatemala, Haiti, Honduras, Jamaica, Martinique, Mexico, Montserrat, Nicaragua, Panama, Puerto Rico, Saint Kitts and Nevis, Saint Lucia, Saint Vincent and the Grenadines, Turks and Caicos Islands, United States Virgin Islands
South America	Developed economies, most with decreasing emissions.	Argentina, Aruba, Bolivia (Plurinational State of), Brazil, Chile, Colombia, Ecuador, Falkland Islands (Malvinas), French Guiana, Grenada, Guyana, Paraguay, Peru, Suriname, Trinidad and Tobago, Uruguay, Venezuela
Sub-Saharan Africa	Developing economies, slightly increasing emissions.	Angola, Benin, Botswana, Burkina Faso, Burundi, Cameroon, Central African Republic (the), Comoros (the), Congo (the), Democratic Republic of the Congo, Equatorial Guinea, Eswatini, Gabon, Ghana, Kenya, Lesotho, Liberia, Madagascar, Malawi, Mauritius, Mayotte, Mozambique, Namibia, Nigeria, Reunión, Rwanda, Seychelles, Sierra Leone, South Africa, United Republic of Tanzania (the), Togo, Uganda, Zambia, Zimbabwe
Northern Africa and Middle East	Developing economies, with increasing emissions.	Algeria, Armenia, Azerbaijan, Bahrain, Cabo Verde, Chad, Cote d'Ivoire, Djibouti, Egypt, Eritrea, Ethiopia, Gambia (the), Georgia, Guinea, Guinea-Bissau, Iran (Islamic Republic of), Iraq, Israel, Jordan, Kuwait, Lebanon, Libyan Arab Jamahiriya, Mali, Mauritania, Morocco, Niger, Oman, Palestine, Qatar, Saint Helena, Sao Tome and Principe, Saudi Arabia, Senegal, Somalia, Sudan, Syria, Tunisia, Turkey, United Arab Emirates, Western Sahara, Yemen
Europe	Developed economies, most with decreasing emissions.	Albania, Andorra, Austria, Belarus, Belgium, Bosnia and Herzegovina, Bulgaria, Channel Islands, Croatia, Cyprus, Czechia, Denmark, Estonia, Faroe Islands, Finland, France, Germany, Gibraltar, Greece, Greenland, Hungary, Iceland, Ireland, Isle of Man, Italy, Latvia, Liechtenstein, Lithuania, Luxembourg, Malta, Montenegro, Netherlands (Kingdom of the), North Macedonia, Norway, Poland, Portugal, Republic of Moldova (the), Romania, Serbia, Slovakia, Slovenia, Spain, Sweden, Switzerland, Ukraine, United Kingdom

Northern Eurasia	Show declining emissions following the break-up of USSR and then slightly increasing trends.	Kazakhstan, Kyrgyzstan, Mongolia, Russian Federation (the), Tajikistan, Turkmenistan, Uzbekistan
East Asia	Strong economies except the Democratic People's Republic of Korea. China shows increasing emissions but levelling off after 2016 while the Republic of Korea and Japan show little change since 2000	China mainland, Hong Kong, Japan, Macao, Democratic People's Republic of Korea, Republic of Korea (the), Taiwan
South and southeast Asia	Developing economies, with increasing emissions.	Afghanistan, Bangladesh, Bhutan, Brunei Darussalam, Cambodia, Cook Islands, Fiji, French Polynesia, Guam, India, Indonesia, Kiribati, Lao People's Democratic Republic (the), Malaysia, Maldives, Marshall Islands (the), Myanmar, Nauru, Nepal, New Caledonia, Niue, Norfolk Islands, Northern Mariana Islands, Pacific Islands Trust Territory, Palau, Papua New Guinea, Philippines (the), Pitcairn, Samoa, Singapore, Solomon Islands, Sri Lanka, Thailand, Timor-Leste, Tokelau, Tonga, Tuvalu, Vanuatu, Viet Nam, Wallis and Futuna Islands
Australasia	Wealthy countries with little change in emissions.	Australia, New Zealand

SI 4 Impacts on climate, air quality and the ozone layer

SI 4.1 Climate and other impacts

Methods: models

Climate and air quality impacts were analysed from simulations with the GISS-E2.1-G composition-climate model as used in CMIP6/AR6 (Kelley *et al.* 2020). This model was driven with changes in prescribed nitrous oxide concentrations evaluated using a simple model of the nitrous oxide-cycle based on an atmospheric residence time of 121 years (IPCC, 2014) and nitrous oxide emissions in the INMS scenarios described in Chapter 2. Changes in associated emissions of nitrogen oxides and methane from those sectors with substantial nitrous oxide emissions, namely agriculture, waste and industry, from those scenarios were also included. Note that those sectors capture nearly all changes in ammonia emissions under these scenarios, whereas for nitrogen oxides they represent just under 30 per cent of total cuts with the rest being largely in the transport, shipping and energy sectors along with a minor contribution from the residential, commercial and other sector. Companion simulations were performed with the GEOS-Chem model (Murray *et al.* 2021) to provide an additional set of air pollution simulations – as a chemistry-transport model, those simulations do not evaluate climate change. Finally, simulations were also performed with the CESM2 model, as used in CMIP6 (Danabasoglu *et al.* 2020). This model provided changes in surface pollutants and radiative forcing due to the imposed scenarios. At the time of writing of this Assessment, only a single ensemble member from that model was completed, so that the radiative forcing results, though consistent with those in the GISS model, were too uncertain to provide a strong constraint. Hence those are not included here, though additional ensemble members will be completed and analysed to provide further characterisation of the climate impact of these scenarios. The surface pollution changes from that model are incorporated in this Assessment. Climate and surface ozone changes projected by the GISS model were used in the China's Climate Change Integrated Assessment Model/Global Energy and Environmental Policy Analysis Model (C3IAM3.0/GEEPA; Wei *et al*. 2021) to evaluate crop yield changes under the three scenarios. Climate, surface ozone and nitrogen deposition changes projected by the GISS model were also used to drive the Community Land Model (CLM) (Boas *et al.* 2021) to examine the carbon cycle response in the three scenarios.

Methods: methane changes

Under SSP2-4.5, total anthropogenic methane emissions are 370 Mt/yr averaged over 2040–2050. Methane emissions for the agricultural sector decrease by 10.7 Mt/yr under technical reductions scenario relative to reference scenario, and by 48.1 Mt/yr under the technical reductions and societal change scenario relative to the reference one. If natural emissions are around 230 Mt/yr, then these decreases in methane emissions represent reductions of 1.8 per cent and 8.0 per cent of total emissions for technical reductions and technical reductions and societal change scenarios, respectively. The response of methane concentrations to these changes are evaluated in methane emissions using the relationship between methane concentrations and emissions derived in prior work (Fiore *et al.* 2008):

$$C'/C = (E'/E)^f$$

where C' and E' are the changed concentrations and emissions, respectively, C and E are the original concentrations and emissions, respectively, and f is the feedback factor. A feedback factor of 1.34 was used as in AR5 (IPCC, 2014). Under technical reductions scenario, the emissions decrease lead to a concentration of 1,746 ppb, whereas under technical reductions and societal change scenario the emissions decrease lead to a concentration of 1,599 ppb. The respective forcings from these changes are evaluated using the SSP2-4.5 estimated nitrous oxide concentration of around 349 ppb for the 2040–2050 period.

Methods: long-term radiative-forcing scenarios

Out to 2100, the SSPs that span a wide range of potential nitrous oxide emissions can be used. By 2100, the nitrous oxide forcing in the SSP database for SSP1-2.6 *versus* SSP2-4.5 is -0.058 W/m², so under this scenario the continued decrease in nitrous oxide relative to the SSP2-4.5 case would provide an additional negative forcing of 0.038 (technical reductions scenario) or 0.031 (technical reductions and societal change scenario) W/m² by 2100. This would reduce the net positive forcing at that time, but under both scenarios, and whether cuts in agricultural methane emissions are or are not accounted for, the forcing would still be positive if other emissions remained the same.

The long-term nitrous oxide forcing reduction only becomes very large in comparison with a very high nitrous oxide emission scenario or using a very low nitrous oxide scenario. The SSP3 baseline has the highest 2100 emissions, and under that scenario the nitrous oxide forcing becomes -0.20 W/m² by 2100 for SSP1-2.6 versus SSP3-7.0 (-0.14 W/m² by 2080). That scenario, however, projects an increase from today's anthropogenic nitrous oxide emissions of about 12 Mt/yr to more than 20 Mt/yr in 2100, which is very large, though perhaps consistent with a continuation of recent trends that have matched or exceeded worst-case scenarios. For context, the middle-of-the-road SSP2-4.5 scenario projects 2100 anthropogenic nitrous oxide emissions of just 9 Mt/yr. SSP3-7.0 also projects anthropogenic nitrous oxide emissions to increase 3.9 Mt/yr between 2020 and 2050 whereas this Assessment's reference scenario has emissions growth of just 2.8 Mt/yr during this period. Within the AR6 (IPCC, 2023) database, examining scenarios with at least 50 per cent chance of keeping temperatures below 1.5° C with no or limited overshoot (termed C1 in AR6) have on average 7.7 Mt/yr anthropogenic nitrous oxide emissions in 2100, so just slightly lower than SSP1-2.6 (8.4 Mt/yr).

For very low anthropogenic nitrous oxide emissions scenarios, the lowest C1 scenario has just 2.5 Mt/yr nitrous oxide emissions in 2100, but that is an extreme case produced by a single Integrated Assessment Model (Prospective Outlook on Long-term Energy Systems (POLES); the next lowest is the Regional Model of Investment and Development (REMIND) with 3.6 Mt/yr). This Assessment's technical reductions and societal change scenario has 5.4 Mt/yr in 2050, whereas the very low POLES scenarios have less than 4 Mt/yr and REMIND has 4.8 Mt/yr in 2050. Those in the AR6 database that are consistent with extension of the technical reductions and societal change scenario, which has anthropogenic nitrous oxide emissions 5.4 Mt/yr in 2050, were examined. The set of scenarios with 4.5–5.8 Mt/yr anthropogenic nitrous oxide emissions in 2050 has a mean of 5.2 Mt/yr, similar to this Assessment's value. Using the mean of those scenarios, emissions decrease by roughly another 1 Mt/yr by 2100.

Methods: health analyses

For the health effects of particulate matter exposure, we first examined the near-present day health effects of fine particulate matter ($PM_{2.5}$) exposure to put the results of this modeling into context was examined first. Using the GEMM (Burnett *et al.* 2018) and 2019 population (CIESIN, FAO and CIAT 2017) and vulnerability (GBD 2021), the 2017–2021 average $PM_{2.5}$ exposure in the GISS model leads to 7.6 million (6.5– 8.6 million; 95 per cent confidence interval (CI)) premature annual deaths for people aged 25 and older. The 2017–2021 average $PM_{2.5}$ exposure in the CESM model leads to 6.3 million (5.5–7.2 million; 95 er cent CI) premature annual deaths for this age group. In comparison, the GEMM paper using a model calibrated to satellite observations of aerosol optical depth finds 8.9 million (7.5–10.3; 95 per cent CI) deaths in 2015. The values in this Assessment being 15 and 28 per cent lower than the result reported in the original GEMM paper for GISS and CESM, respectively, are similar to the uncertainty of around ±27 per cent in global annual premature deaths due to $PM_{2.5}$ exposure calculated with GEMM using inputs based on different sets of observation-based data (Parsons *et al.* 2023). The reasonable agreement between this Assessment's model and analyses using observation is consistent with multiple prior comparisons of the GISS model's simulated $PM_{2.5}$ with observed values (Shindell *et al.* 2021; 2022; 2024). Similarly, using the $PM_{2.5}$ simulated by the GEOS-Chem model for 2015 8.9 million annual premature deaths (7.7–10.0 million; 95 per cent CI) deaths were found, matching GEMM.

For the health effects of ozone exposure, first the model performance for ozone was evaluated. Comparisons over a large portion of the world, based on the 5,264 monitoring stations assembled in the global hidden ozone structure (GHOST project) (Bowdalo *et al.* 2024), combined with data from China's Beijing Municipal Environmental Monitoring Center/China National Environmental Monitoring Center (acquired at http:// beijingair.sinaapp.com) show a positive bias of 16.6 per cent in GISS ozone for 2018. A scale factor of 0.834 was therefore applied to debias the model output. To test the suitability of this scaling, the respiratory deaths associated with the 2015 modelled ozone values were compared with those previously evaluated using statistically infilled dense observational networks in China, Europe and the US (Seltzer, Shindell and Malley 2018). Results show that using the scaled GISS model's ozone leads to a positive bias of 5.8 per cent, well within the uncertainty associated with the exposure-response function. It was noted that biases in the GEOS-Chem model for 2018 in comparison with the same data were 35 per cent, so that surface ozone changes from this Assessment's model were not used in its health impact analysis. Results from CESM for present-day are very similar to those from the debiased GISS analysis, so that the ozone output from that model was used without debiasing. Note, however, that the model has substantial differences over parts of Africa and India, as discussed in the main text, where little evaluation data is available.

Using Turner *et al.* (2016) epidemiology and 2019 population and vulnerability data, the number of premature annual deaths globally for people aged 30 and older based on the 2017–2021 average ozone is 1.88 million (1.03–2.66 million; 95 per cent CI). Of these, 940,000 (670,000–1,190,000) per year result from respiratory diseases. These are widely included in ozone-health analyses as they have the most robust evidence base, whereas cardiovascular diseases and diabetes have greater uncertainties and are therefore less often incorporated. Prior work (Seltzer, Shindell and Malley 2018) has shown that use of the Turner *et al.* (2016) exposure-response function, based on an extended version of the American Cancer Society Cancer Prevention Study-II (ACS CPS-II) dataset, produces 1.5 to 2 times as many deaths as the older ACS CPS-II analysis of Jerrett *et al.* (2009) commonly used in benefit analyses. Hence the mid-range estimate of 940,000 respiratory global deaths reported here would correspond to around 470,000–630,000 respiratory deaths using the older epidemiology, a value slightly higher than the 365,000 estimated by GBD for 2019. The low-range 670,000 of the estimate used here would, however, correspond to values of around 255,000–340,000 using the older epidemiology, so that range here overlaps the GBD's while this Assessment's central estimates are higher.

The benefits of the decreased $PM_{2.5}$-related premature deaths was monetised using a willingness-to-pay measure of the value societies place upon reduced risk of premature death. This well-established metric from the economics literature is drawn from both stated and revealed preference studies and applicable globally (Viscusi and Aldy 2003; OECD 2016). The US Environmental Protection Agency's value of a statistical life for 2018 was used, with a cross-country income elasticity of 1.0 (World Bank and IHME 2016) and national income levels from the World Bank (2020).

Methods: carbon-cycle response

Carbon-cycle responses are based on running the CLM with input carbon dioxide from SSP2-4.5 and input surface ozone and nitrogen deposition from the GISS and GEOS-Chem models. The nitrogen deposition tends to be biased low in both models (Figures SI 4.1 and 4.2), so that impacts of changes in those fluxes are likely conservative. This Assessment explored the use of two different models to represent ecosystem responses to ozone exposure, Lombardozzi *et al.* (2015) and Li *et al.* (2024).

Responses of nitrous oxide emissions are not directly taken from CLM. Instead, this Assessment first used soil nitrous oxide emissions in the 2010s simulated by eight terrestrial biosphere models (Tian *et al.* 2024) and total nitrogen inputs for land, including nitrogen fixation, fertilisation, and deposition, from the CLM model in 2010–2014 to calculate the nitrous oxide-emission factor relative to total nitrogen input for each grid cell. It was assumed that this soil nitrous oxide-emission factor remains constant over time. Using the land nitrogen input data of CLM under different scenarios in the future, combined with this emission factor, the changes of nitrous oxide emissions from all soils, including croplands, was estimated.

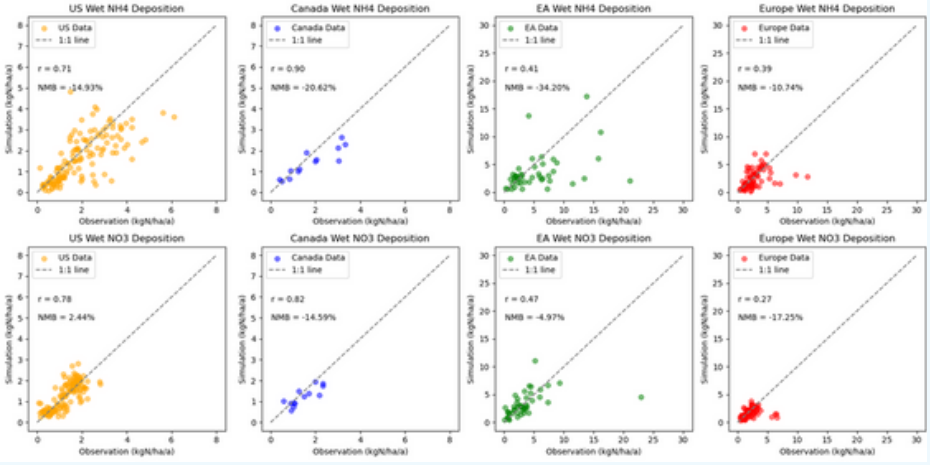

Figure SI 4.2 *GISS model relative to observations, 2015, kilograms of nitrogen per hectare per year.*

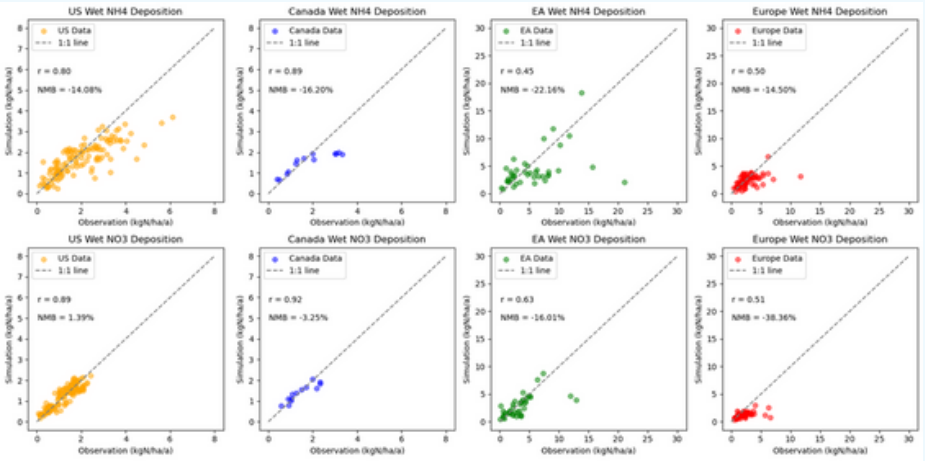

Figure SI 4.2 *GEOS-Chem model relative to observations, 2015, kilograms of nitrogen per hectare per year. Note: EA = East Asia*

Methods: crop-yield responses

Crop-yield changes in percentages for barley, maize, rice and wheat are based on a climate-crop-yield meta-analysis (Challinor *et al.* 2014) and ozone-crop-yield response relationships (Mills *et al.* 2018). The study uses the local temperature, precipitation and ozone results of the GISS simulations as inputs to calculate the percentage crop-yield changes in grid-scale yields under different scenarios. The results are mapped on to the crop area of different crops (Monfreda, Ramankutty and Foley 2008) to calculate the percentage change for four main crop-yield changes at national and regional scales. The total production change from 2045–2050 is calculated based on the trend of historical harvest area and crop yields in the FAO database (FAO 2022).

Results: crop-yield responses

The average changes are the most significant for wheat (94,000 t and 104,000 t for the technical reductions scenario versus the reference and technical reductions and societal change scenarios versus the reference scenario, respectively. The average changes for rice are 69,000 t and 78,000 t at the global level. For India, the total crop yields of rice increase significantly to 580,000 t and 774,000 t and the total crop-yields of wheat increase by 742,000 t and 890,000 t under the comparison between technical reductions regulation *versus* the reference scenario and the technical reductions and societal change *versus* the reference scenario, respectively. Wheat in China also shows significant increases of 219,000 t and 230,000 t under the comparison between the technical reductions scenario regulation versus the reference and technical reductions and societal change scenarios versus the reference scenario, respectively.

SI 4.1 Nitrous oxide, stratospheric ozone depletion and its impact

Description of the NASA/Goddard Space Flight Center 2-D Mode

The NASA/Goddard Space Flight Center two-dimensional (2D) model (GSFC2D) has been used extensively in chemistry-climate coupling studies of the stratosphere and mesosphere, as well as the WMO/UNEP ozone assessments (WMO 2022). The model has detailed stratospheric chemistry and reduced tropospheric chemistry, with a diurnal cycle computed for all constituents each day. The model domain extends from the surface to about 92 kilometres (0.002 hectopascals (hPa)) with a grid spacing of 4° latitude and 1 km in altitude. The latest Jet Propulsion Laboratory (JPL) 2019 recommendations (Burkholder *et al.* 2019) are used for the kinetic reaction rates, photolysis cross sections, and heterogeneous reactions on the surfaces of PSCs and stratospheric sulphate aerosols. A detailed description and evaluation of the model has been provided recently (Fleming *et al.* 2024).

Description of the chemistry-climate models

Two comprehensive chemistry-climate models were used: (1) CESM version 2; and (2) CMAM.

The first is the CESM2 (Danabasoglu *et al.* 2020) with the WACCM version 6 (Gettelman *et al.* 2019) using a detailed interactive troposphere-stratosphere-mesosphere-lower-thermosphere chemistry scheme and MAM 4 for both the tropospheric and stratospheric aerosols. The simulations were run in a fully-coupled atmosphere-ocean configuration, i.e., with interactive ocean at 0.9º latitude by 1.25º longitude atmospheric horizontal resolution and 70 vertical levels up to around 140 km.

The second is the CMAM from the Canadian Centre for Climate Modelling and Analysis (CCCma). The CMAM is based on a vertically extended version of the third generation Canadian Atmospheric General Circulation model (Scinocca *et al.* 2008) and is run at T47

horizontal resolution with 80 levels between the ground and approximately 95 km. The model contains a comprehensive description of stratospheric chemistry, including the long-lived bromine- and chlorine-containing halocarbons, nitrous oxide, methane, and the inorganic chemistry of ClO_x, BrO_x, NO_x, HO_x and O_x compounds. The version of CMAM used for these simulations is not coupled to an ocean model and requires specified sea-surface temperatures and sea-ice, provided as monthly average fields taken from a simulation of the fourth generation CCCma coupled atmosphere-ocean general circulation model (GCM).

The results from the two chemistry-climate models and the two-dimensional model were compared with model output from CCMI-1 (Morgenstern *et al.* 2017). CCMI-1 used greenhouse gas forcing scenarios from the older CMIP5. Namely, the base scenario is the RCP6.0 (Hijioka *et al.* 2008). The $\delta(O_3)/\delta(N_2O)$ values for 2100 for the CCMI-1 models by comparing RCP6.0 to sensitivity simulations in which nitrous oxide is held at its 1960 value while other concentrations follow RCP6.0 (Hegglin *et al.* 2016). Details of this analysis are described in Morgenstern *et al.* (2018).

Sensitivity of ozone to nitrous oxide across models

Following Morgenstern *et al.* (2018), we obtained the quantity $F = \delta(O_3)/\delta(N_2O)$ through regression of the modelled results. This method assumes that ozone responds linearly to nitrous oxide changes at the surface and that the delay in the ozone response due to the transport of the nitrous oxide signal from the surface to the stratosphere can be ignored. An additional assumption is that the ozone response to nitrous oxide is not sensitive to differences in the background scenarios for methane, carbon dioxide and potentially the ODSs. This coefficient *F* is shown in Figure SI 4.3 for the three models used in this Assessment. CESM2, CMAM and GSFC2D are generally consistent, giving similar sensitivities of total column ozone to nitrous oxide.

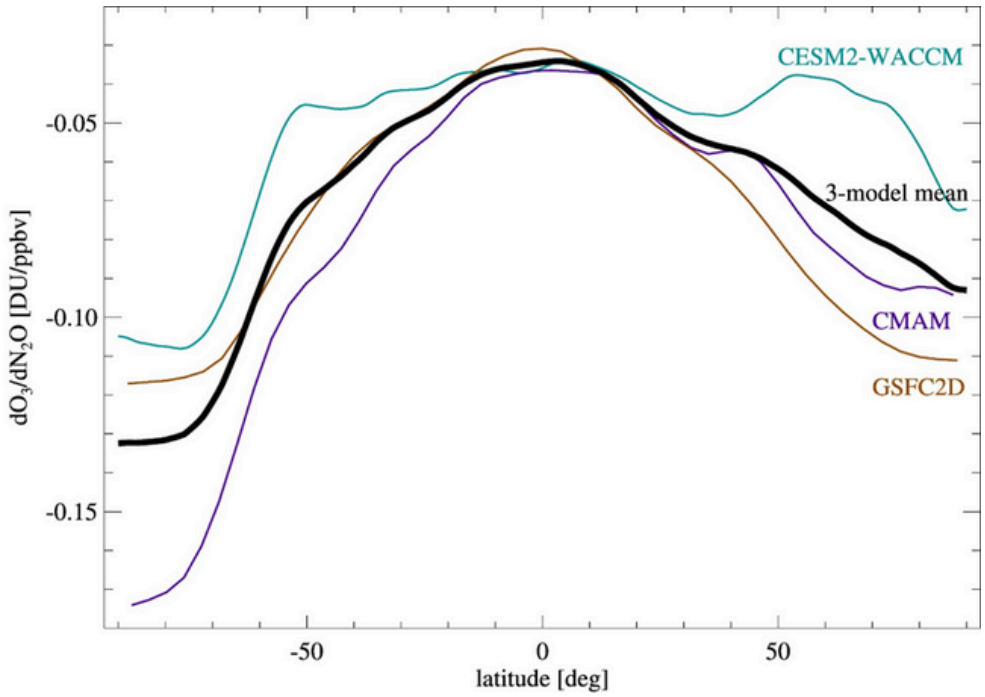

Figure SI 4.3 *Total-column ozone sensitivities to differences in the nitrous oxide mixing ratio, F, in Dobson Units of ozone per parts per billion by volume (DU/ppbv) of nitrous oxide, calculated using the SSP1-2.6 CO_2/CH_4 +SSP3-7.0 nitrous oxide scenario relative to the SSP1-2.6 scenario from 2020–2100. Note: the black solid line represents the mean of the three models shown in the figure. For comparison to values calculated from CCMI models, see Morgenstern et al. (2018).*

Figure SI 4.4 shows the sensitivity, *F*, of vertically resolved ozone to surface nitrous oxide. The three models agree with previously published CCMI1 results (Morgenstern *et al.* 2018) in that the response is composed of decreases in ozone in the middle stratosphere (the leading influence) and offsetting smaller ozone increases in the lower stratosphere. CESM2-WACCM simulates larger compensating increases at middle and high latitudes, giving a smaller decrease in total-column ozone in the extratropics than GSFC2D (Figure SI 4.4). CMAM restricts the offsetting to the tropics and has negative trends throughout the stratosphere at southern high latitudes, giving an overall larger ozone depletion in response to nitrous oxide increases than CESM2-WACCM and GSFC2D. GSFC2D disagrees with CESM2-WACCM and CMAM on the sign of the mesospheric response (above 1 hPa, a small effect). Similar disagreements also exist in the CCMI1 ensemble (Morgenstern *et al.* 2018). The GSFC2D simulations indicate that the climate scenario only has a relatively minor influence on these results. This small signal is consistent with the finding that for CESM2-WACCM and CMAM, the results are very similar to the CCMI1 results derived from older versions of these models assuming a different climate scenario, vindicating the approach taken here of expressing the ozone response as simply proportional to the assumed differences in surface nitrous oxide.

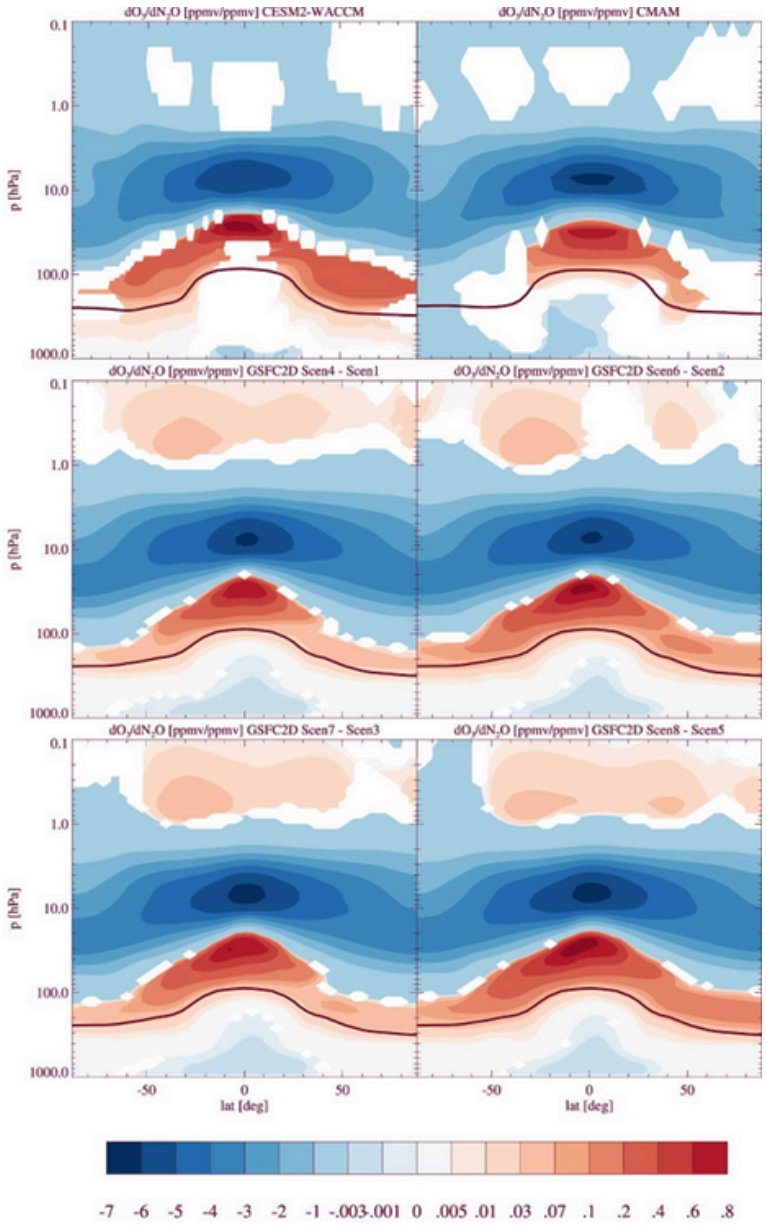

Figure SI 4.4 *Sensitivity (F) of zonal- and annual-mean ozone to surface nitrous oxide (parts per million by volume [ppmv] of ozone/ppmv of nitrous oxide), where nitrous oxide follows the SSP370 and SSP126 scenarios, respectively*
Note: white patches: Insignificant changes at 68% confidence.
Top left: CESM2-WACCM. Top right: CMAM. Other panels: GSFC2D nitrous oxide sensitivity values for different scenarios. (Scen 4 - Scen 1) = (N_2O SSP3-7.0+CO_2/CH_4 SSP1-2.6) - (all SSP1-2.6); (Scen 6 - Scen 2) = (N_2O/CH_4 SSP3-7.0+CO_2 SSP1-2.6) - (N_2O/CO_2 SSP1-2.6+CH_4 SSP3-7.0); (Scen 7 - Scen 3) = (N_2O/CO_2 SSP3-7.0+CH_4 SSP1-2.6) - (N_2O/CH_2 SSP1-2.6+CO_2 SSP3-7.0); (Scen 8 - Scen 5) = (all SSP3-7.0) - (CO_2/CH_4 SSP3-7.0+N_2O SSP1-2.6). Bold contour: mean position of the ozone tropopause (i.e., the 150 ppbv of ozone contour) in the SSP1-2.6 scenario simulations.

Additional sensitivity tests by individually varying greenhouse gas trajectories

Sensitivity tests were performed with the GSFC2D. Global-mean mixing ratio boundary conditions of carbon dioxide, methane and nitrous oxide were systematically perturbed one at a time towards the evolution of different SSP scenarios, to isolate the influence of individual gases on the global-mean total column ozone. Table SI 4.1 shows the sensitivity tests that were performed.

Table SI 4.1 *Sensitivity experiments performed with the GSFC2D model*
Note: here the numbers refer to different SSP scenario trajectories for nitrous oxide, carbon dioxide and methane: 1.9 = SSP1-1.9 (strong mitigation scenario), 2.6 = SSP1-2.6 (mitigation scenario), 4.5 = SSP2-4.5 (middle-of-the-road scenario), 7.0 = SSP3-7.0 (unmitigated scenario).

Scenario	Nitrous oxide	Carbon dioxide	Methane
SSP1-2.6	2.6	2.6	2.6
SSP2-4.5	4.5	4.5	4.5
SSP3-7.0	7.0	7.0	7.0
Unmitigated nitrous oxide	7.0	2.6	2.6
Unmitigated methane	2.6	2.6	7.0
Unmitigated carbon dioxide	2.6	7.0	2.6
Mitigated nitrous oxide only	2.6	7.0	7.0
Mitigated carbon dioxide only	7.0	2.6	7.0
Mitigated methane only	7.0	7.0	2.6
Mitigated nitrous oxide, middle-of-the-road carbon dioxide + methane	2.6	4.5	4.5
Middle-of-the-road nitrous oxide, strongly mitigated carbon dioxide + methane	4.5	1.9	1.9
Unmitigated nitrous oxide, strongly mitigated carbon dioxide + methane	7.0	1.9	1.9
Unmitigated nitrous oxide, middle-of-the-road carbon dioxide + methane	7.0	4.5	4.5

Additional sensitivity tests with GSFC 2D were done to compare the effects of mitigating nitrous oxide with the actions taken by the Montreal Protocol to accelerate the phasedown of HCFCs. In these experiments, we compare nitrous oxide mitigation scenarios (e.g., reducing nitrous oxide from SSP2-4.5 and SSP3-7.0 trajectories to SSP1-2.6) to a case in which HCFC-22 follows either future projections assumed in the baseline scenario of the 2006 WMO ozone assessment report, or in the 2010 WMO ozone assessment report in which projections included an accelerated phasedown. HCFC-141b and HCFC-142b were not altered in the calculation because of differences in the projections due to issues other than the accelerated phaseout. The results are shown in Figure 4.10 and in Table SI 4.2.

Figure SI4.5 shows the effects on globally-averaged ozone of individually modifying the trajectory of carbon dioxide, methane, and nitrous oxide to either a high emissions scenario (SSP3-7.0) or a low emissions scenario (SSP1-2.6), while the other two gases follow a medium emissions scenario (SSP2-4.5).

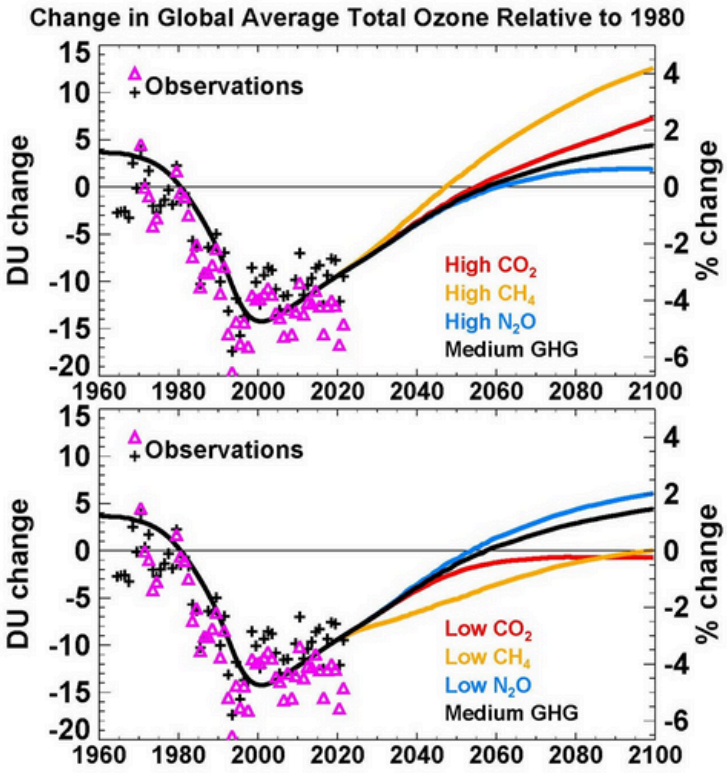

Figure SI 4.5 Change in globally-averaged total column ozone relative to 1980, for scenarios in which carbon dioxide, methane and nitrous oxide trajectories are individually modified to (above) follow the high-emissions scenario, or (lower) follow the low-emissions scenario, while the other two gasses are kept at the middle-of-the-road (medium) greenhouse gas scenario, 1960–2100, change in Dobson units (left) and per cent (right). Note: the observations are from satellite (magenta triangles) and ground-based (black crosses) platforms (Weber et al. 2022).

Table SI 4.2 Global total column ozone changes from Figure SI 4.3 integrated over the time periods indicated
Note: included are nitrous oxide mitigation (SSP1-1.9 minus SSP2-4.5 and SSP1-1.9 minus SSP3-7.0, respectively), and HCFC accelerated phasedown (using HCFC projections from the 2010 WMO Ozone assessment with accelerated phasedown minus HCFC projections from the 2006 WMO Ozone assessment).

	Low nitrous oxide mitigation	Strong nitrous oxide mitigation	HCFC-22 benefit
2020-2050	0.24 DU (0.08%)	0.33 (0.12%)	0.18 DU (0.06%)
2020-2070	0.53 DU (0.19%)	0.84 DU (0.29%)	0.22 (0.08%)
2020-2100	0.92 (0.32%)	1.82 (0.63%)	0.16 DU (0.05%)

Changes in ozone for scenario in which carbon dioxide and methane are mitigated but nitrous oxide is not, across all models

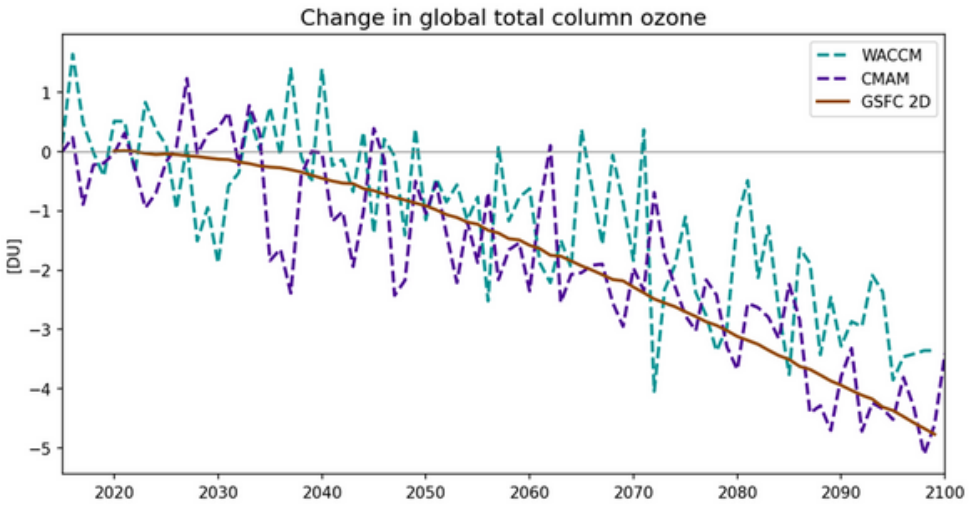

Figure SI 4.6 *Time series of the change in globally-averaged ozone for the scenario in which carbon dioxide and methane follow the SSP1-2.6 scenario while nitrous oxide follows SSP3-7.0, relative to the SSP1-2.6 scenario, 2020-2100, Dobson units.*

Calculation of Biologically active UV radiation for the induction of skin cancer.

The biologically active UV radiation, E_{bio}, is obtained by integrating over wavelength λ the spectral irradiance $E(\lambda)$ weighted by a sensitivity function, or action spectrum, $w(\lambda)$.

$$E_{bio} = \int_{280\,nm}^{400\,nm} E(\lambda)w(\lambda)d\lambda$$

For the induction of skin cancer the Skin Cancer Utrecht Philadelphia (SCUP-h) action spectrum for cancers is used as in previous studies (van Dijk *et al.* 2013; Madronich *et al.* 2021). It is based on laboratory measurements on mice, corrected for human skin transmission (de Gruijl *et al.* 1993; van der Leun, Piacentini and de Gruijl 2008), $E(\lambda)$ depends also on solar zenith angle, i.e., on latitude, season, and time of day; aerosols; surface albedo and clouds. Here $E(\lambda)$ was calculated with the TUV radiative transfer model (Madronich, 1993) in 15-minute steps for the 15th day of each month and for the middle latitude of five latitude bands. For computational expedience, only E_{bio} for cloud-free skies and typical values of aerosols and surface albedo as a function of month (m) and latitude (lat) for one reference year were calculated. Then a simple power-scaling relation to estimate the effect of total ozone column (TOC) perturbations in subsequent years was supplied:

$$E_{bio}(year, lat, m) = E_{bio}(year_{ref}, lat, m)\left(\frac{TOC(year, lat, m)}{TOC(year_{ref}, lat, m)}\right)^{-RAF}$$

where RAF is the so-called Radiation Amplification Factor, defined as:

$$RAF = -\frac{\Delta E_{bio} / E_{bio}}{\Delta TOC / TOC}$$

This scaling has been shown to be accurate, compared to full radiative transfer calculations, for action spectra that decrease exponentially with increasing wavelengths

n the 300–330 nanometre (nm) region, as is true for the SCUP-h spectrum (Micheletti, Piacentini and Madronich 2003; McKenzie *et al.* 2022). Tabulations of RAFs are available (McKenzie et *al.* 2011), and a value of 1.2 appropriate for the SCUP-h action spectrum is used here.

The biologically active radiation E_{bio} is calculated for each month to account for the natural seasonality of UV radiation and the total ozone column. The monthly values are summed to obtain annual UV exposures used in estimating the health effects. The calculation of E_{bio} for the period of study is based on TOC simulated by three different models, CMAM, WACCM and 2D, and for two different scenarios: SSP1-2.6 (as the reference scenario) and SSP1-2.6 with nitrous oxide from SSP3-7.0 (perturbation scenario).

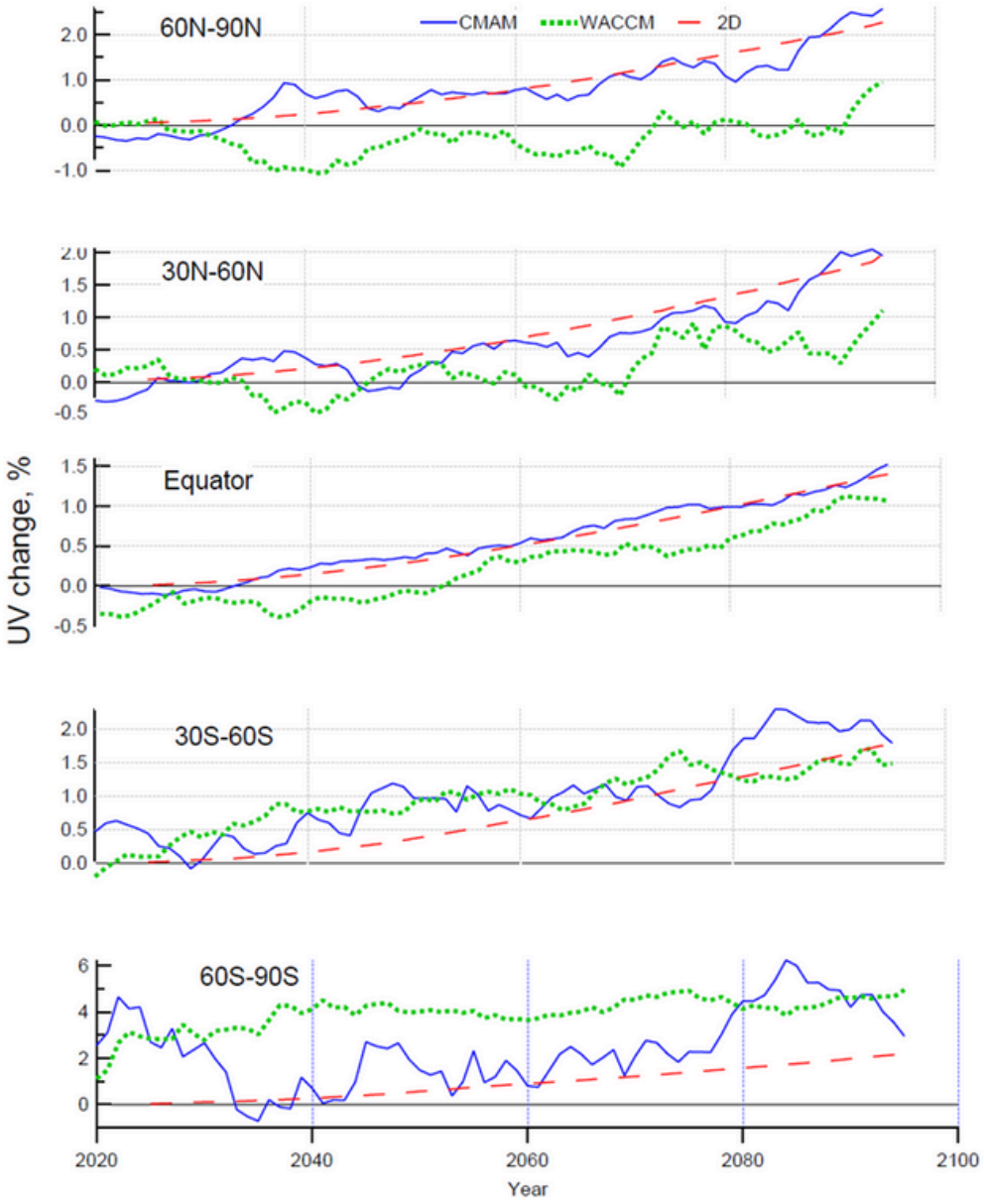

Figure SI 4.7 *Percent difference in annual skin cancer-inducing ultraviolet radiation, for the SSP1-2.6 with nitrous oxide from SSP3-7.0 scenario relative to the SSP1-2.6 scenario for five different latitude bands, 2020–2100, per cent.*
Note: estimates are 11-year running averages based on total ozone simulations by three climate models.

The changes in annual E_{bio} can be used to estimate the consequent changes in the incidence, SCI, of UV-induced skin cancers and cataracts. Previous studies (Madronich and de Gruijl 1993; van der Leun, Piacentini and de Gruijl 2008; van Dijk *et al.* 2013; Madronich *et al.* 2021) have parameterised this dependence with a power dose-response relation:

$$BAF = -\frac{\Delta SCI / SCI}{\Delta E_{bio} / E_{bio}}$$

where BAF is the biological amplification factor, determined from geographic and epidemiologic data. Values of BAF have been estimated as approximately 1.4±0.4 for squamous cell carcinoma (SCC) and 2.5±0.7 for basal cell carcinoma (BCC) (Madronich and de Gruijl, 1993; de Gruijl and Forbes, 1995), 0.6±0.4 for cutaneous malignant melanoma (CMM) (de Gruijl and Forbes 1995; van Dijk *et al.* 2013), and 0.2±0.1 for cataracts (West *et al.* 1998). Table SI 4.3 illustrates the application of these BAF values to the UV changes (from Table 4.5) calculated for 2085. Of note is that these estimates do not include many factors, such as future changes in cloud cover and aerosols, occupational and recreational exposure patterns, demographic shifts or disease latency.

Table SI 4.3 *Approximate changes in health impacts due to simulated changes in UV radiation, E_{bio} , in the unmitigated nitrous oxide scenario, 2085, per cent*

Health impact change (%)	90° S – 60° S	60° S – 30° S	30° S – 30° N	30° N – 60° N	30° N – 60° N
Squamous cell carcinoma	9.8	4.2	2.5	2.5	2.2
Basal cell carcinoma	5.5	2.4	1.4	1.4	1.3
Cutaneous malignant melanoma	2.3	1.0	0.6	0.6	0.5
Cataracts	0.8	0.3	0.2	0.2	0.2

SI 4.3 Gender-associated impacts of climate change, air pollution and ozone depletion

Changes in annual UV irradiances associated with the depletion of the stratospheric ozone have differing health effects depending on gender. Zhang *et al.* (2021) found that men have a higher age-standardised rate than women. The estimated age standardised incidence per 100,000 people per year of invasive cutaneous melanoma was 3.8 for men and 3.0 for women, while the cumulative risk of developing melanoma (birth to age 74 years, globally) is estimated to be 0.39 per cent in men and 0.31 per cent in women (noting that this is an average of the markedly different risks in people with light and dark skin) (Neale *et al.* 2023).

While gender-based differences in vulnerability to ambient air pollution have not been widely explored (Liu *et al.* 2020), studies suggest that health responses may differ between women and men and between girls and boys (Clougherty 2010). Women, for example, tend to be more vulnerable to the adverse health effects of tropospheric ozone (O_3) exposure. Climate change impacts also differ for men and women, largely as a result of and amplification of existing gender dynamics – with women being disproportionately negatively affected (UN Women 2022).

The CCAC recognises that while climate change and air pollution affect all people, women and girls are more vulnerable to these effects due to persisting gender inequalities, gender discrimination, and social exclusion. These inequities may be intensified by additional dimensions of social disadvantage. Gender, including non-binary identities, intersects with factors such as race, class, socio-economic status, nationality, education, migrant status, religion, and disability, producing multidimensional inequalities and amplifying social vulnerability.

SI 5 Implementing nitrous oxide abatement measures

Table SI 5.1 *Detailed descriptions of nitrous oxide abatement measures in China.*

Measures	Description	Mitigation potential	Reference
Advanced emission control technologies	Install and utilise advanced emission control tehcnologies, such as selective catalytic reduction (SCR) or thermal destruction systems during industrial processes, especially for chemical industry.	80-90 %	Davidson and Winiwarter (2023); Alves *et al.* (2022)
Upgrade vehicle emissions standards	Implementing stricter regulations on vehicle emissions, especially for heavy-duty vehicles and diesel engines, can contribute to significant emission reductions.	60-70 %	Kanter *et al.* (2013); Wallington and Wiesen (2014)
Process optimisation and waste reduction	Optimise raw material selection and implement advanced manufacturing processes to reduce waste and improve resource management, especially for the chemical industry.	60-80 %	Davidson and Winiwater(2023); Winiwarter *et al.* (2018)
Use renewable energy	Promote the installation of renewable energy systems such as solar panels or small wind turbines for household electricity generation. Utilising cleaner energy sources reduces dependence on fossil fuels while reducing nitrous oxide emissions from biomass open burning.	50-80 %	Feng and Li (2023)
Wastewater management	Promote water conservation and improve household water treatment rates; optimise the disposal process to improve the N_2/N_2O ratio of the effluent.	40-60 %	Feng and Li (2023)
Reforestation	High nitrogen fertiliser inputs can lead to large soil NO emissions and returning famland to forest or reforestation can weaken nitrous oxide emissions to some extent.	20-30 %	Feng and Li (2023)
Apply ultra-low technologies	Promote the ultra-low emission technologies and utilise tertiary abatement technologies in the chemical industry, where the nitrous oxide decomposition unit is installed after the nitrogen oxides absorption tower and the exhaust nitrous oxide is discharged downstream after nitrogen oxides absorption.	60-80 %	Hasanbeigi and Sibal (2023); Li, Hu and Han (2014)

Promote electric vehicles	Encouraging the adoption of electric vehicles (EVs) can significantly reduce GHG emissions from transportation. China has already been promoting electric mobility, continued support for EV infrastructure development, incentives for EV purchases.	60-80 %	Meng *et al.* (2023)
Soil/crop management	Adopt cropland soil or crop management practices to control soil nitrification and denitrification, including adjusting tillage intensity and frequency, using cover crops, and applying organic amendments.	24-38 %	Yin *et al.* (2024); Xia *et al.*(2017)
Animal management	Adjusting livestock stocks to match available forage and resources; and selective breeding to improve productivity and feed conversion efficiency.	30-50 %	Kanter, Ogle and Winiwarter (2020)
Improved irrigation	Improved irrigation practices could optimise nitrogen use efficiency, conserve energy, and promote soil health.	10-40 %	Grados *et al.* (2022)
Improve fuel quality and productivity	During energy production, utilise an afterburner to raise the temperature in the flue gas to destroy nitrous oxide and reverse air classification is used to optimise the availability of oxygen. Besides, coal washing, blending and sorting, upgrading combustion systems, turbines, boilers and generators to newer models that have better fuel efficiency ratings.	80-90 %	Winiwarter *et al.* (2018)
Manure management	Manure management practices include solid-liquid separation, manure cover storage, acidifying slurry by additives, promoting faeces composting and anaerobic digestion to convert faeces into organic fertilizers, and promoting the fermentation of faeces to produce biogas.	20-50 %	Xu *et al.* (2022); Houe, Velthof and Oenema (2015)
Enhance public transportation	Expanding and improving public transportation systems can reduce the number of private vehicles on the road. Investments in high-capacity buses, metro systems, and rail networks can provide more sustainable transportation options, leading to lower nitrous oxide emissions	20-30 %	Meng *et al.* (2023)
Improve fuel efficiency	Combustion at elevated temperatures (800-1,200 K) lead to nitrous oxide formation, from N2 and O2. Improve energy efficiency during industrial combustion by implementing technologies such as cogeneration, heat recovery, and efficient equipment.	80-90 %	Davidson and Winiwarter (2023); Winiwarter *et al.* (2018)
4R fertilisation	The 4R stands for the right source, right rate, right time, and right place of fertiliser application, which enhances nutrient use efficiency, reduces fertiliser waste, and supports crop productivity while minimising the negative consequences of excessive application.	20-40 %	Xia *et al.* (2017)

Feeding and housing adaptation	Implementing a low-crude protein diet and use of additives can improve feed efficiency and reduce methane emissions from enteric fermentation; improved ventilation systems, proper insulation, and optimised space utilisation can help minimise nitrous oxide emissions from animal housing.	6-24 %	Xu *et al.* (2022)
Regulate biomass burning	Promoting sustainable biomass utilisation and cleaner biomass burning practices while enforcing emission limits can help minimise nitrous oxide emissions.	10-20 %	Kanter *et al.* (2013); Shi *et al.* (2023)
Grazing management	Grazing management Rotational grazing, rest periods for vegetation recovery and promoting diverse plant species can improve carbon sequestration and enhance the overall health of grasslands, leading to potential reductions in nitrous oxide emissions.	10-20 %	Rafique, Hennessy and Kiely (2011)

SI References

Alves, L., Holz, L.I., Fernades, C., Ribeirinha, P., Mendes, D., Fagg, D.P. *et al.* (2022). A comprehensive review of NO_x and N_2O mitigation from industrial streams. *Renewable and Sustainable Energy Reviews*, 155, 111916. https://doi.org/10.1016/j.rser.2021.111916.

Ball, B.C., Horgan, G.W. and Parker, J.P. (2000) Short-range spatial variation of nitrous oxide fluxes in relation to compaction and straw residues. *European Journal of Soil Science,* 51, 607–616. https://doi.org/10.1046/j.1365-2389.2000.00347.x.

Boas, T., Bogena, H., Grünwald, T., Heinesch, B., Ryu, D., Schmidt, M. *et al*. (2021). Improving the representation of cropland sites in the Community Land Model (CLM) version 5.0. *Geoscientific Model*, 14(1), 573–601. https://doi.org/10.5194/gmd-14-573-2021.

Bowdalo, D., Basart, S., Guevara, M., Jorba, O., Pérez García-Pando, C., Jaimes Palomera, M. *et al.* (2024). GHOST: A globally harmonised dataset of surface atmospheric composition measurements. *Earth System Science Data Discussions*, 1–137. https://doi.org/10.5194/essd-16-4417-2024.

Burkholder, J.B., Sander, S.P., Abbatt, J., Barker, J.R., Cappa, C., Crounse, J.D. *et al*. (2019). *Chemical Kinetics and Photochemical Data for Use in Atmospheric Studies: Evaluation No. 19. JPL Publication 19-5*. Pasadena: Jet Propulsion Laboratory. http://jpldataeval.jpl.nasa.gov.

Burnett, R., Chen, H., Szyszkowicz, M., Fann, N., Hubbell, B., Pope, C.A. 3rd *et al*. (2018). Global estimates of mortality associated with long-term exposure to outdoor fine particulate matter. *Proceedings of the National Academy of Sciences of the United States of America*, 115, 9592–9597. https://doi.org/10.1073/pnas.1803222115.

Butterbach-Bahl, K., Baggs, E.M., Dannenmann, M., Kiese, R. and Zechmeister-Boltenstern, S. (2013). Nitrous oxide emissions from soils: How well do we understand the processes and their controls? Transactions of the Royal Society B: Biological Sciences, 368(1621), 20130122. https://doi.org/10.1098/rstb.2013.0122.

Butterbach-Bahl, K., Rothe, A. and Papen, H. (2002). Effect of tree distance on nitrous oxide and CH_4-fluxes from soils in temperate forest ecosystems. *Plant and Soil,* 240, 91–103. https://www.jstor.org/stable/24122622.

Chalinel, R., Jean-Luc Attié, J-L., Philippe Ricaud, P., Vidot, J., Kangah, Y., Hauglustaine, D. *et al.* (2022). Evaluation and global-scale observation of nitrous oxide from IASI on Metop-A. *Remote Sensing (Basel),* 14(6), 1403. https://doi.org/10.3390/rs14061403.

Challinor, A.J., Watson, J., Lobell, D.B., Howden, S.M., Smith, D.R. and Chhetri, N. (2014). A meta-analysis of crop yield under climate change and adaptation. *Nature Climate Change*, 4, 287–291. https://doi.org/10.1038/nclimate2153.

CIESIN, FAO and CIAT (2017). *Gridded population of the World: Future estimates, 2017 (GPWv4): Population grids*. Available from http://sedac.ciesin.columbia.edu/gpw.

Clougherty, J.E. (2010). A growing role for gender analysis in air pollution epidemiology. *Ciência & Saúde Coletiva,* 118, 167–176. https://doi.org/10.1289/ehp.0900994.

Cui, X., Zhou, F., Ciais, P., Davidson, E.A., Tubiello, F.N., Niu, X. *et al.* (2021) Global mapping of crop-specific emission factors highlights hotspots of nitrous oxide mitigation. *Nature Food*, 2, 886–893. https://doi.org/10.1038/s43016-021-00384-9.

Danabasoglu, G., Lamarque, J-F., Bacmeister, J., Bailey, D.A., DuVivier, A.K., Edwards, J. *et al.* (2020). The Community Earth System Model Version 2 (CESM2). *Journal of Advances in Modeling Earth Systems*, 12(2), e2019MS001916. https://doi.org/10.1029/2019MS001916.

Davidson, E.A. and Winiwarter W. (2023). Urgent abatement of industrial sources of nitrous oxide. *Nature Climate Change*, 13, 599–601. https://doi.org/10.1038/s41558-023-01723-3.

van Dijk A., Slaper H., den Outer P. N., Morgenstern O., Braesicke P., Pyle, J.A. *et al.* (2013). Skin cancer risks avoided by the Montreal Protocol--worldwide modeling integrating coupled climate-chemistry models with a risk model for UV. *Photochemistry and Photobiology*, 89(1), 234–246. https://doi.org/10.1111/j.1751-1097.2012.01223.x.

Eagle, A.J., McLellan, E.L., Brawner, E.L., Chantigny, M.H., Davidson, E.A., Dickey, J.B. *et al.* (2020). Quantifying on-farm nitrous oxide emission reductions in food supply chains. *Earth's Future*, 8(10), e2020EF001504. https://doi.org/10.1029/2020EF001504.

Eugster, W., Zeyer, K., Zeeman, M., Michna, P., Zingg, A., Buchmann, N. *et al.* (2007) Methodical study of nitrous oxide eddy covariance measurements using quantum cascade laser spectrometery over a Swiss forest. *Biogeosciences*, 4(5), 927–939. https://doi.org/10.5194/bg-4-927-2007.

Feng, R. and Li, Z. (2023) Current investigations on global N_2O emissions and reductions: Prospect and outlook. Environmental Pollution, 338(6557), 122664. https://doi.org/10.1016/j.envpol.2023.122664.

Fiore, A.M., West, J.J., Horowitz, L.W., Naik, V. and Schwarzkopf, M.D (2008). Characterizing the tropospheric ozone response to methane emission controls and the benefits to climate and air quality. *Journal of Geophysical Research*, 113, D08307. https://doi.org/10.1029/2007JD009162.

Fleming, E.L., Newman, P.A., Liang, Q. and Oman, L.D. (2024). Stratospheric temperature and ozone impacts of the Hunga Tonga-Hunga Ha'apai water vapor injection. *Journal of Geophysical Research: Atmospheres,* 129(1), e2023JD039298. https://doi.org/10.1029/2023JD039298.

Food and Agriculture Organization of the United Nations (2022). FAOSTAT Statistical Database. https://www.fao.org/faostat/en/#data.

Gettelman, A., Mills, M. J., Kinnison, D. E., Garcia, R. R., Smith, A. K., Marsh, D.R. *et al*. (2019). The Whole Atmosphere Community Climate Model Version 6 (WACCM6). *Journal of Geophysical Research: Atmospheres*, 124(23), 12380–12403. https://doi.org/10.1029/2019JD030943.

Global Burden of Disease Collaborative Network (2021). Global Burden of Disease Study 2019 (GBD 2019), Air Pollution Exposure Estimates 1990–2019. Seattle: Institute for Health Metrics and Evaluation 2021. https://doi.org/10.6069/70JS-NC54.

Grados D., Butterbach-Bahl, K., Chen, J., van Groenigen, K.J., Olesen, J.E., van Groenigen, J.W. *et al.* (2022). Synthesising the evidence of nitrous oxide mitigation practices in agroecosystems. *Environmental Research Letters*, 17, 114024. https://doi.org/10.1088/1748-9326/ac9b50.

de Gruijl, F.R. and Forbes, P.D. (1995). UV-induced skin cancer in a hairless mouse model. *BioEssays*, 17(7), 651–660. https://doi.org/10.1002/bies.950170711.

de Gruijl, F.R., Sterenborg, H.J.C.M., Forbes, P.D., Davies, R.E., Cole, C., Kelfkens, G. *et al*. (1993). Wavelength dependence of skin cancer induction by ultraviolet irradiation of albino hairless mice. *Cancer Research*, 53(1), 53–60. https://aacrjournals.org/cancerres/article/53/1/53/498742/Wavelength-Dependence-of-Skin-Cancer-Induction-by.

Hasanbeigi, A. and Sibal, A (2023). *Stopping a Super-pollutant: N_2O Emissions Abatement from Global Adipic Acid Production*. Florida, United States: Global Efficiency Intelligence. https://go.nature.com/3pgzhFg.

Hegglin, M. I., Lamarque, J.-F., Duncan, B., Eyring, V., Gettelman, A., Hess, G. *et al.* (2016). Report on the IGAC/SPARC Chemistry-Climate Model Initiative (CCMI) 2015 science workshop. *SPARC Newsletter*, 46, 37–42.

Hijioka, Y., Matsuoka, Y., Nishimoto, H., Masui, M. and Kainuma, M. (2008). Global GHG emissions scenarios under GHG concentration stabilization targets. *Journal of Global Environmental Engineering*, 13, 97–108. https://doi.org/10.1111/gcb.12767.

Hou, Y., Velthof, G.L. and Oenema, O. (2015). Mitigation of ammonia, nitrous oxide and methane emissions from manure management chains: a meta-analysis and integrated assessment. *Global Change Biology*, 21(3), 1293–1312.

Huang, J., Golombek, A., Prinn, R., Weiss, R., Fraser, P., Simmonds, P. *et al.* (2008). Estimation of regional emissions of nitrous oxide from 1997 to 2005 using multinetwork measurements, a chemical transport model, and an inverse method. *Journal of Geophysical Research*, 113, D17313.

Intergovernmental Panel on Climate Change (2014). *Climate Change 2014: Synthesis Report. Contribution of Working Groups I, II and III to the Fifth Assessment Report of the Intergovernmental Panel on Climate Change*. Core Writing Team, Pachauri, R.K. and Meyer, L.A. (eds.) Geneva: Intergovernmental Panel on Climate Change. https://www.ipcc.ch/report/ar5/syr.

Intergovernmental Panel on Climate Change (2023). *Climate Change 2023: Synthesis Report. Contribution of Working Groups I, II and III to the Sixth Assessment Report of the Intergovernmental Panel on Climate Change*. Core Writing Team, Lee, H. and Romero, J. (eds.). Geneva: Intergovernmental Panel on Climate Change. https://www.ipcc.ch/report/sixth-assessment-report-cycle.

Jerrett, M., Burnett, R.T., Pope III, C.A., Ito, K., Thurston, G., Krewski, D. *et al.* (2009). Long-term ozone exposure and mortality. *New England Journal of Medicine*, 360, 1085–1095. https://doi.org/10.1056/NEJMoa0803894 .

Kangah, Y., Ricaud, P., Attié, J-L., Saitoh, N., Hauglustaine, D.A., Wang, R. *et al.* (2017). Summertime upper tropospheric nitrous oxide over the Mediterranean as a footprint of Asian emissions. *Journal of Geophysical Research: Atmospheres*, 122(8), 4746–4759. https://doi.org/10.1002/2016JD026119.

Kanter, D., Mauzerall, D.L., Ravishankara, A.R., Daniel, J.S., Portmann, R.W., Grabiel, P.M. et al. (2013). A post-Kyoto partner: Considering the stratospheric ozone regime as a tool to manage nitrous oxide. Proceedings of the National Academy of Sciences of the USA, 110(12), 4451–4457. https://doi.org/10.1073/pnas.1222231110.

Kanter, D.R., Ogle, S.M. and Winiwarter, W. (2020). Building on Paris: integrating nitrous oxide mitigation into future climate policy. Current Opinion in Environmental Sustainability, 47, 7–12. https://doi.org/10.1016/j.cosust.2020.04.005.

Kelley, M., Schmidt, G.A., Nazarenko, L.S., Bauer, S.E., Ruedy, R., Russell, G.L. *et al*. (2020). GISS-E2.1: Configurations and climatology. *Journal of Advances in Modeling Earth Systems*, 12(8), e2019MS002025. https://doi.org/10.1029/2019MS002025.

Lebegue, B., Schmidt, M., Ramonet, M., Wastine, B., Yver Kwok, C., Laurent, O. *et al*. (2016). Comparison of nitrous oxide (N_2O) analyzers for high-precision measurements of atmospheric mole fractions. *Atmospheric Measurement Techniques*, 9(3), 1221–1238. https://doi.org/10.5194/amt-9-1221-2016.

van der Leun J. C., Piacentini R. D. and de Gruijl F. R. (2008). Climate change and human skin cancer. *Photochemical & Photobiological Sciences*, 7(6), 730-733. https://doi.org/10.1039/B719302E.

Li, L., Xu, J., Hu, J. and Han, J. (2014). Reducing nitrous oxide emissions to mitigate climate change and protect the ozone layer. *Environmental Science and Technology Journal*, 48(9), 5290–5297. https://doi.org/10.1021/es404728s.

Li, F., Zhou, Z., Levis, S., Sitch, S., Hayes, F., Feng, Z. *et al*. (2024). Quantifying the role of ozone-caused damage to vegetation in the Earth system: A new parameterization scheme for photosynthetic and stomatal responses. *Geoscientific Model Development Discussions*, 17(16), 6173–6193. https://doi.org/10.5194/gmd-17-6173-2024.

Liu, G., Sun, B., Yu, L., Chen, J., Han, B., Li, Y. *et al*. (2020). The gender-based differences in vulnerability to ambient air pollution and cerebrovascular disease mortality: Evidences based on 26781 deaths. *Global Heart*, 15(1), 46. https://doi.org/10.5334/gh.849.

Lombardozzi, D., Levis, S., Bonan, G., Hess, P. and Sparks, J. (2015). The influence of chronic ozone exposure on global carbon and water cycles. *Journal of Climate*, 28, 292–305. https://doi.org/10.1175/JCLI-D-14-00223.1.

Madronich, S. (1993). UV Radiation in the Natural and Perturbed Atmosphere. In *Environmental Effects of UV (Ultraviolet) Radiation*. Tevini, M. (ed.). Boca Raton: Lewis Publishers.

Madronich, S. and de Gruijl, F.R. (1993). Skin cancer and UV radiation. *Nature*, 366, 23. https://doi.org/10.1038/366023a0.

Madronich, S., Lee-Taylor, J.M., Wagner, M., Kyle, J., Hu, Z. and Landolfi, R. (2021). Estimation of skin and ocular damage avoided in the United States through implementation of the Montreal Protocol on substances that deplete the ozone layer. *ACS Earth and Space Chemistry*, 5(8), 1876–1888. https://doi.org/10.1021/acsearthspacechem.1c00183.

McKenzie, R.L., Aucamp, P.J., Bais, A.F., Bjoern, L.O., Ilyas, M. and Madronich, S. *et al.* (2011). Ozone depletion and climate change: impacts on UV radiation. *Photochemical & Photobiological Sciences*, 10(2), 182–198. https://doi.org/10.1039/c0pp90034f.

McKenzie R., Liley B., Kotkamp M., Geddes A., Querel R., Stierle, S. *et al.* (2022). Relationship between ozone and biologically relevant UV at 4 NDACC sites. *Photochemical & Photobiological Sciences,* 21, 2095–2114. https://doi.org/10.1007/s43630-022-00281-5.

Meng, Z., Yan, Li, K., Gao, J. and Zhang, B. (2023). Revealing non-CO_2 GHG emissions in China's transportation networks. *Environmental Science and Technology Letters*, 10(2), 124–130. https://doi.org/10.1021/acs.estlett.2c00832.

Micheletti M., Piacentini R. and Madronich S. (2003). Sensitivity of biologically active UV radiation to stratospheric ozone changes: Effects of action spectrum shape and wavelength range. *Photochemistry and Photobiology*, 78(5), 456–461. https://doi.org/10.1562/0031-8655(2003)078%3C0456:sobaur%3E2.0.co;2.

Mills, G., Sharps, K., Simpson, D., Pleijel, H., Frei, M., Burkey, K. *et al*. (2018). Closing the global ozone yield gap: Quantification and cobenefits for multistress tolerance. *Global Change Biology*, 24(10), 4869–4893. https://doi.org/10.1111/gcb.14381.

Monfreda, C., Ramankutty, N. and Foley, J.A (2008). Farming the planet: 2. Geographic distribution of crop areas, yields, physiological types, and net primary production in the year 2000. *Global Biogeochemical Cycles*, 22.

Morgenstern, O., Hegglin, M. I., Rozanov, E., O'Connor, F. M., Abraham, N. L., Akiyoshi, H. *et al.* (2017). Review of the global models used within phase 1 of the Chemistry–Climate Model Initiative (CCMI). *Geoscientific Model Development*, 10(2), 639–671. https://doi.org/10.5194/gmd-10-639-2017.

Morgenstern, O., Stone, K. A., Schofield, R., Akiyoshi, H., Yamashita, Y., Kinnison, D.E. *et al.* (2018). Ozone sensitivity to varying greenhouse gases and ozone-depleting substances in CCMI-1 simulations. *Atmospheric Chemistry and Physics*, 18(2), 1091–1114. https://doi.org/10.5194/acp-18-1091-2018.

Murray, L.T., Leibensperger, E.M., Orbe, C., Mickley, L.J. and Sulprizio, M (2021). GCAP 2.0: a global 3-D chemical-transport model framework for past, present, and future climate scenarios. G*eoscientific Model Development*, 14(9), 5789–5823. https://doi.org/10.5194/gmd-14-5789-2021.

Neale, R.E., Lucas, R.M., Byne, S.N., Hollestein, L., Rhodes, L.E., Yazar, S. *et al.* (2023). The effects of exposure to solar radiation on human health. *Photochemical & Photobiological Sciences,* 22(5), 1011-1047. https://doi.org/10.007/s43630-023-00375-8.

Organisation for Economic Co-operation and Development [OECD] (2016). *The economic consequences of outdoor air pollution.* OECD, Paris. http://doi.org/10.1787/9789264257474-en.

Parsons, L., Shindell, D., Faluvegi, G. and Nagamoto, E. (2023). Geophysical uncertainties in air pollution exposure and benefits of emissions reductions for global health. Earth's Future, 11(9), e2023EF003839. https://doi.org/10.1029/2023EF003839.

Rafique, R., Hennessy, D. and Kiely, G. (2011). Nitrous oxide emission from grazed grassland under different management systems. *Ecosystems*, 14, 563–582. http://dx.doi.org/10.1007/s10021-011-9434-x.

Saikawa, E., Schlosser, C.A. and Prinn, R.G. (2013). Global modeling of soil nitrous oxide emissions from natural processes. *Global Biogeochemical Cycles*, 27(3), 972–989. https://doi.org/10.1002/gbc.20087.

Scinocca, J. F., McFarlane, N. A., Lazare, M., Li, J. and Plummer, D. (2008). Technical note: The CCCma third generation AGCM and its extension into the middle atmosphere. *Atmospheric Chemistry and Physics*, 8(23), 7055–7074. https://doi.org/10.5194/acp-8-7055-2008.

Seltzer, K.M., Shindell, D.T. and Malley, C. (2018). Measurement-based assessment of health burdens from long-term ozone exposure in the United States, Europe, and China. *Environmental Research Letters*, 13, 104018. https://doi.org/10.1088/1748-9326/aae29d.

Shcherbak, I., Millar, N. and Robertson, G.P. (2014). Global metaanalysis of the nonlinear response of soil nitrous oxide (N_2O) emissions to fertilizer nitrogen. *Proceedings of the National Academy of Sciences of the United States of America*, 111(25), 9199–9204. https://doi.org/10.1073/pnas.1322434111.

Shi, W., Fang, Y.R., Chang, Y. and Xie, G.H. (2023). Toward sustainable utilization of crop straw: Greenhouse gas emissions and their reduction potential from 1950 to 2021 in China. Resources, Conservation and Recycling, 190, 106824.

Shindell, D., Ru, M., Zhang, Y., Seltzer, K., Faluvegi, G., Nazarenko, L. *et al*. (2021). Temporal and spatial distribution of health, labor and crop benefits of climate change mitigation in the US. *Proceedings of the National Academy of Sciences of the USA*, 118(46), e2104061118. https://doi.org/10.1073/pnas.2104061118.

Shindell, D., Faluvegi, G., Parsons, L., Nagamoto, E. and Chang, J. (2022). Premature deaths in Africa due to particulate matter under high and low warming scenarios. *GeoHealth*, 6(5), e2022GH000601. https://doi.org/10.1029/2022GH000601.

Shindell, D., Faluvegi, G., Nagamoto, E., Parsons, L. and Zhang, Y. (2024). Reductions in premature deaths from heat and particulate matter air pollution in South Asia, China, and the US under decarbonization. *PNAS*, 121(5), e2312832120. https://doi.org/10.1073/pnas.2312832120.

Thompson, R. L., Chevallier, F., Crotwell, A.M., Dutton, G., Langenfelds, R.L., Prinn, R.G. *et al*. (2014). Nitrous oxide emissions 1999 to 2009 from a global atmospheric inversion. *Atmospheric Chemistry and Physics*, 14, 1801–1817. https://doi.org/10.5194/acp-14-1801-2014.

Tian, H., Pan, N., Thompson, R.L., Canadell, J.G., Suntharalingam, P., Regnier, P. *et al*. (2024). Global nitrous oxide budget (1980–2020). *Earth System Science Data*, 16(6), 2543–2604. https://doi.org/10.5194/essd-16-2543-2024.

Tian, H., Yang, J., Xu, R., Lu, C., Canadell, J.G., Davidson, E.A. *et al*. (2019) Global soil nitrous oxide emissions since the pre-industrial era estimated by an ensemble of Terrestrial Biosphere Models: Magnitude, attribution and uncertainty. *Global Change Biology*, 25(2), 640–659. https://doi.org/10.1111/gcb.14514.

Turner, M.C., Jerrett, M., Pope III, C.A., Krewski, D., Gapstur, S.M., Diver, W.R. *et al*. (2016). Long-term ozone exposure and mortality in a large prospective study. *American Journal of Respiratory and Critical Care Medicine*, 193(10), 1134–1142. https://doi.org/10.1164/rccm.201508-1633OC.

UN Women (2022). *Explainer: How Gender Inequality and Climate Change are Interconnected*. https://www.unwomen.org/en/news-stories/explainer/2022/02/explainer-how-gender-inequality-and-climate-change-are-interconnected. Accessed October 2024.

Viscusi, W.K. and Aldy, J.E. (2003). The value of a statistical life: A critical review of market estimates throughout the world. *Journal of Risk and Uncertainty,* 27, 5–76. https://doi.org/10.1023/A:1025598106257

Wallington, T.J. and Wiesen, P. (2014). N_2O emissions from global transportation. *Atmospheric Environment*, 94, 258–263. https://doi.org/10.1016/j.atmosenv.2014.05.018.

Weber, M., Arosio, C., Coldewey-Egbers, M., Fioletov, V.E., Frith, S.M., Wild, J.D. *et al.* (2022). Global total ozone recovery trends derived from five merged ozone datasets. *Atmospheric Chemistry and Physics*, 22(10), 6843–6859. https://doi.org/10.5194/acp-22-6843-2022.

Wei, Y-M., Liu, L-J., Liang, Q-M., Yu, B-Y., Liu, L-C., Yao, Y-F. *et al*. (2021). Pathway comparison of limiting global warming to 2C. *Energy and Climate Change*, 2, 100063. https://doi.org/10.1016/j.egycc.2021.100063.

Weiss, R.F. (1981). Determinations of carbon dioxide and methane by dual catalyst flame ionization chromatography and nitrous oxide by electron capture chromatography. *Journal of Chromatographic Science,* 19(12), 611–616. https://doi.org/10.1093/chromsci/19.12.611.

West, S.K., Duncan, D.D., Munoz, B., Rubin, G.S., Fried, L.P., Bandeen-Roche, K. et al. (1998). Sunlight exposure and risk of lens opacities in a population-based study: the Salisbury Eye Evaluation project. JAMA, 280(8), 714-718. https://doi.org/10.1001/jama.280.8.714.

Winiwarter, W., Höglund-Isaksson, L., Klimont, Z., Schöpp, W. and Amann, M. (2018). Technical opportunities to reduce global anthropogenic emissions of nitrous oxide. *Environmental Research Letters*, 13, 14011. https://doi.org/10.1088/1748-9326/aa9ec9.

World Bank (2020). *World development indicators.* World Bank Group, Washington, DC. https://databank.worldbank.org/source/world-development-indicators

World Bank and Institute for Health Metrics and Evaluation [IMHE] (2016). *The cost of air pollution: Strengthening the economic case for action.* World Bank Group, Washington, DC. http://documents.worldbank.org/curated/en/781521473177013155/The-cost-of-air-pollution-strengthening-the-economic-case-for-action

World Meteorological Organization (2007). *Scientific Assessment of Ozone Depletion: 2006*. Global Ozone Research and Monitoring Project – Report No. 50. Geneva: WMO.

World Meteorological Organization. (2011). *Scientific Assessment of Ozone Depletion: 2010*. Global Ozone Research and Monitoring Project – Report No. 52. Geneva: WMO.

World Meteorological Organization (2022). *Scientific Assessment of Ozone Depletion: 2022*, GAW Report No. 278. Geneva: WMO.

Xia, L., Lam, S.K., Chen, D., Wang, J., Tang, Q. and Yan, X. (2017). Can knowledge-based N management produce more staple grain with lower greenhouse gas emission and reactive nitrogen pollution? A meta-analysis. *Global Change Biology*, 23(5), 1917–1925. https://doi.org/10.1111/gcb.13455.

Xu, P., Houlton, B.Z., Zheng, Y., Zhou, F., Ma, L., Li, B. *et al*. (2022). Policy-enabled stabilization of nitrous oxide emissions from livestock production in China over 1978–2017. *Nature Food*, 3, 356–366. https://doi.org/10.1038/s43016-022-00513-y.

Yin, W., Chai, Q., Fan, Z, Hu, F., Zhao, L., Fan, H. *et al.* (2024) Agricultural management could reduce soil N2O emissions while increasing grain yields via enhancing soil moisture harvesting and improving soil nutrient status. *CATENA*, 242, 108088. https://doi.org/10.1016/j.catena.2024.108088.

Zhang, W., Zeng, W., Jiang, A., He, Z., Shen, X., Dong, X. et al. (2021). Global, regional and national incidence, mortality and disability-adjusted life-years of skin cancers and trend analysis from 1990 to 2019: An analysis of the Global Burden of Disease Study 2019. *Cancer Medicine*, 10(14), 4905–4922. https://doi.org/10.1002/cam4.4046.